ACS APPLIED MATERIALS & INTERFACES

www.acsami.org

Research Article

Closed-Loop Nanopatterning of Liquids with Dip-Pen Nanolithography

Verda Saygin, Bowen Xu, Sean B. Andersson, and Keith A. Brown*

Cite This: https://doi.org/10.1021/acsami.1c00095

Read Online

ACCESS | Metrics & More | Article Recommendations | Supporting Information

ABSTRACT: The ability to reliably manipulate small quantities of liquids is the backbone of high-throughput chemistry, but the continual drive for miniaturization necessitates creativity in how nanoscale samples of liquids are handled. Here, we describe a closed-loop method for patterning liquid samples on pL to sub-fL scales using scanning probe lithography. Specifically, we employ tipless scanning probes and identify liquid properties that enable probe−sample transport that is readily tuned using probe withdrawal speed. Subsequently, we introduce a novel two-harmonic inertial sensing scheme for tracking the mass of liquid on the probe. Finally, this is combined with a fluid mechanics-based iterative control scheme that selects printing conditions to meet a target feature mass to enable closed-loop patterning with better than 1% accuracy and ∼4% precision in terms of mass. Taken together, these advances address a pervasive issue in scanning probe lithography, namely, real-time closed-loop control over patterning, and position scanning probe lithography of liquids as a candidate for the robust nanoscale manipulation of liquids for advanced high-throughput chemistry.

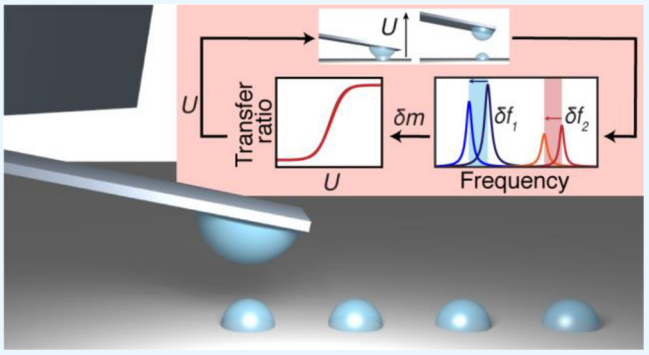

KEYWORDS: *scanning probe lithography, dip-pen nanolithography, nanopatterning, closed-loop, nanoreactor*

1. INTRODUCTION

High-throughput experimentation in chemistry and biology allows researchers to simultaneously perform thousands of experiments in an automated fashion by leveraging miniaturization to reduce reaction volumes and reagent quantities.[1] Microtiter plates are the leading platform for performing such experiments and have evolved from each plate having 96 wells that each hold ∼200 μL to each plate having >3000 wells each with a typical working volume of a few μL. Despite this impressive miniaturization and the discoveries that it has enabled, researchers are still often overwhelmed by the number of potential materials to study. For example, there are estimated to be $\sim 10^{60}$ small organic molecules that have relevance for drug discovery.[2] Thus, the continued miniaturization of liquid volumes is of paramount importance.

Motivated by this desire to handle and deposit ever smaller volumes of liquids and chemicals, researchers have explored scanning probes to write materials with high, and in some cases unsurpassed, resolution. Specifically, dip-pen nanolithography (DPN) comprises an approach to directly write myriad materials ranging from small molecules,[3,4] biological materials,[5] nanoparticles,[6,7] and polymers.[8−10] Significantly, DPN has been used to pattern liquids at the sub-aL scale, with liquid features as small as 15 nm having been demonstrated.[11] Despite the small size of features written by this approach, the method exhibits a major limitation in that it is not currently possible to precisely predict the size of a given feature. This lack of control stems from material transfer depending on a number of environmental conditions, liquid properties, the amount of liquid on the probe, and details of how the probe is programmed to interact with the surface. One potential path to overcoming these limitations is to use information about the state of the probe to adjust writing parameters.[10,12,13] A possible process for gaining such information about the state of the probe is to use changes in the vibrational resonance frequency of the cantilever to determine the mass of liquid on the probe.[14,15] However, adoption of this process has been stymied because it requires a discrete drop of liquid at a well-defined location for quantitative analysis, which precludes the conventional hydrophilic probes with conical tips that are often used for DPN as they exhibit uncontrolled wetting of the liquid on the probe.[15] While this can be reconciled by using hydrophobic probes, drops of liquid on conical probes have no stable configuration at which they can exhibit reliable contact with the surface; they either sit on the side of the probe in a clamshell configuration or, if large enough

Received: January 3, 2021
Accepted: March 5, 2021

to engulf the conical probe, are pushed by surface tension toward the base of the cone.[16] These challenges have prevented DPN of liquids from achieving closed-loop and programmable patterning.

In this report, we present a method for closed-loop control over the liquid written using DPN that overcomes these challenges by combining a novel process for quantifying the liquid on a cantilever, the utilization of a tipless probe architecture, and a control strategy for updating writing parameters *in situ* (Figure 1). Initially, we describe the selection

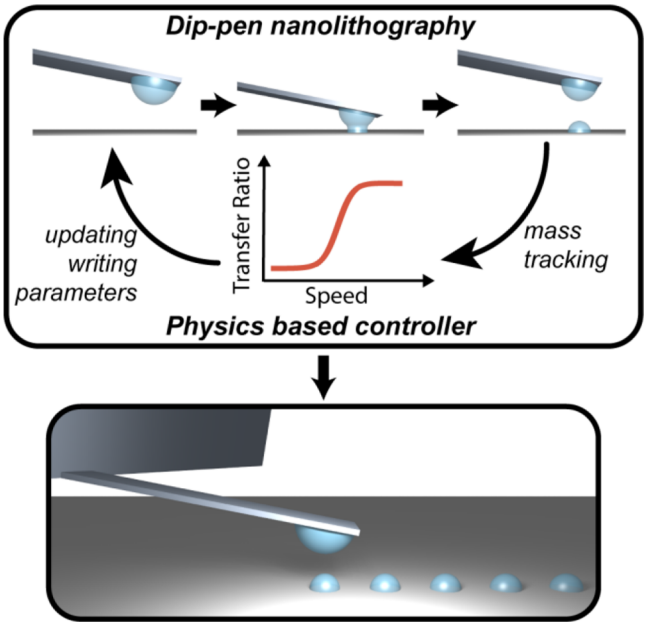

Figure 1. Schematic showing how mass tracking and a physics-based model of liquid transfer can be used together with a tipless atomic force microscope (AFM) probe to realize closed-loop dip-pen nanolithography (DPN).

of a tipless probe that enables robust contact between the liquid and substrate along with model liquids to serve as nonvolatile inks for patterning. Next, we describe a two-mode inertial sensing scheme to simultaneously measure the amount and location of liquid on a cantilever and, when used before and after a transfer operation, quantify the amount deposited with precision approaching the fL scale. This capability allows us to investigate the fundamental characteristics of liquid transport at this scale and identify conditions under which the fraction of liquid transferred from the probe to the substrate is only a function of cantilever withdrawal speed. Using this discovery, we realize predictive control over patterning and develop a closed-loop process for writing patterns with better than 1% accuracy and ~4% precision in terms of liquid mass. Given the versatility of scanning probes to characterize materials once they are written, this work lays the foundation for multifunctional research systems in which chemical experiments are set up, performed, and evaluated at the nanometer scale.

2. RESULTS AND DISCUSSION

The first step toward closed-loop patterning is identifying a probe and liquid system that will provide reliable and quantifiable material transport. We hypothesize that by studying a pendant drop on a nonwetting tipless cantilever, robust contact between a discrete drop and the patterning surface can, in principle, be guaranteed. Removing the conical probe traditionally used in DPN avoids any complications associated with how the drop wets the tip that can otherwise lead to the drop being trapped in a position that precludes liquid contact between the probe and sample (Figure S1). The requirement for a stable pendant drop of liquid means that the liquid must exhibit a few specific, albeit not uncommon, properties. First, to maximize the height of the pendant drop on the cantilever relative to its diameter, the surface tension of the liquid should be large, indicating that oils are not ideal choices as they may wet the cantilever. Additionally, the liquid should be nonvolatile if mass tracking of transferred features during experiments is desired (Figure S3). It should be noted that this particular criterion is perhaps not as important for general patterning tasks where the liquid serves as a vehicle to transfer functional materials but is of high importance here when studying the transport process itself. We select two polymeric liquids that meet these criteria, namely, polyisobutylene (PIB) with a molecular weight of 1500 Da and polyethylene glycol diacrylate (PEGDA) with a molecular weight of 700 Da.

While a tipless probe with a single pendant drop provides a simple fluidic environment for patterning, the lack of a conical probe means that the liquid drop is not pinned at a specific location. This is a challenge because prior work quantifying liquid mass m_l using a mass-spring model relies on the center of m_l being fixed at a known position near the end of the cantilever. When the location of pendant drop is fixed and known, m_l can be calculated by measuring a single quantity, namely, the shift in the first vibrational resonance frequency f_1. Building on prior work from the inertial sensing community,[17] we hypothesized that measuring the shift of two vibrational resonance modes would allow us to determine the drop position (i.e., the location of drop center mass) x in addition to m_l. Specifically, if $m_l \ll M$, with cantilever mass M, the time-independent mode shape function $N_n(x)$ will not be affected by the presence of the liquid and the change in vibrational resonance frequency δf_n of the nth mode of the drop−cantilever system can be approximated as

$$\delta f_n = f_n\left[1 + \frac{m_l}{M}N_n^2(x/L)\right]^{-1/2} - f_n \tag{1}$$

where f_n is the nth vibrational resonance frequency of the cantilever prior to liquid loading and L is the length of the cantilever. By definition, each N_n is normalized such that $\int_0^1 N_n^2(y)\mathrm{d}y = 1$. Practically, it is useful to solve eq 1 to find m_l,

$$m_l = \frac{M}{N_n^2(x/L)}\left[1 - \left(\frac{\delta f_n}{f_n} + 1\right)^{-2}\right] \tag{2}$$

Since there are two unknowns (i.e., m_l and x/L), a minimum of two measurements are needed to determine both.

In order to explore this cantilever bending model as an inertial sensing scheme, we performed a series of experiments with drops of nonvolatile liquids on tipless probes. In particular, we selected a rectangular cantilever with $f_1 \approx 80$ kHz to ensure that the first two modes would be in the frequency range of the instrument as $f_2 \approx 6.3\, f_1$. Initially, the thermal power spectral density (PSD) was measured to find f_1 = 80.382 kHz and f_2 = 504.947 kHz. These measurements, together with a calibration of the optical lever sensitivity, allowed us to compute k = 2.81 N/m and M = 44.065 ng (see the Supporting Information). Subsequently, the probe was positioned over a microliter-scale

https://doi.org/10.1021/acsami.1c00095
ACS Appl. Mater. Interfaces XXXX, XXX, XXX−XXX

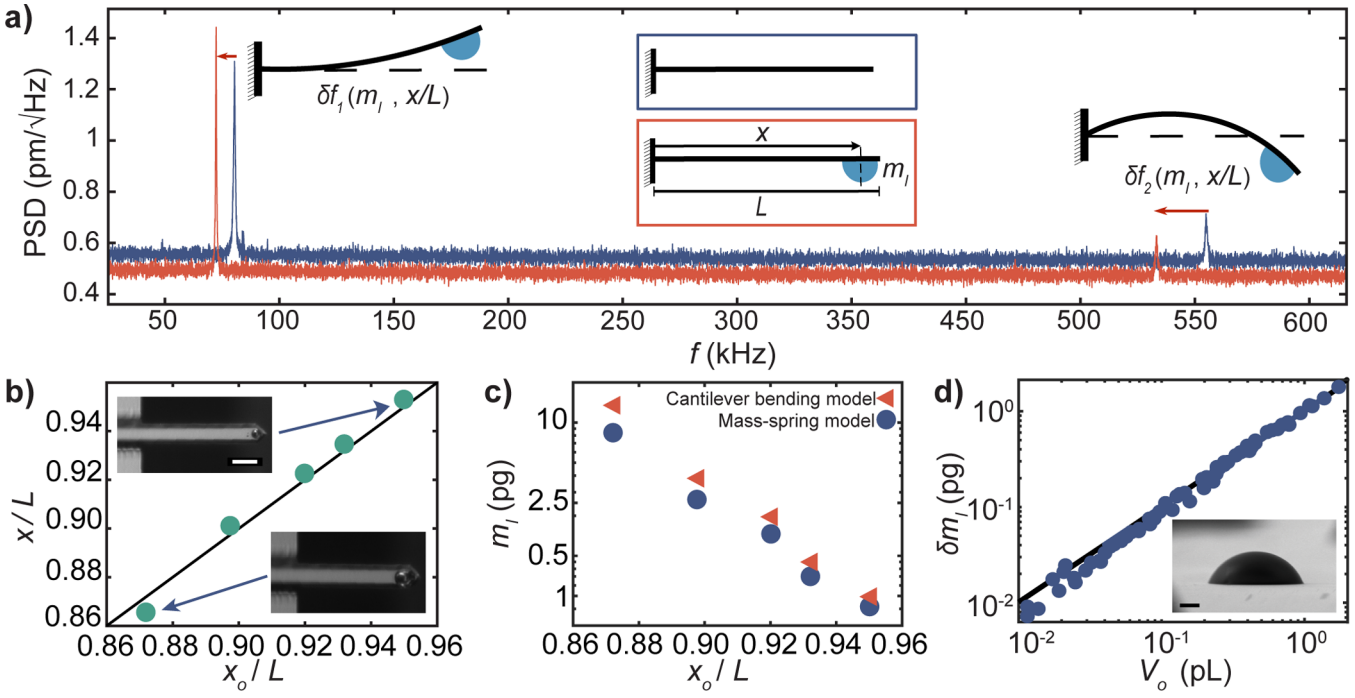

Figure 2. Scheme for measuring the mass of liquid on a cantilever. (a) Measurements of a thermal power spectral density (PSD) vs frequency f that show the first two vibrational resonance modes of a cantilever of length L. Upon loading the cantilever with a drop of liquid with mass m_l at location x, both modes shift to lower frequencies with characteristic shifts δf_1 and δf_2 that depend on both m_l and x/L. (b) Validation of the two-harmonic model for identifying drop location through a comparison of x found by inertial sensing to position x_o determined by inspection using optical microscopy. Insets show optical micrographs of two probe conditions with a 50 μm scale bar. (c) Comparison of m_l predicted by the bending model, which utilizes two harmonics and a mass-spring model that only uses the principal harmonic. (d) Validation of the mass sensing ability of the cantilever bending model through a comparison between the inertially determined transferred liquid mass δm_l and the patterned feature volume V_o determined using optical microscopy. The inset shows an electron micrograph used to compute the contact angle of polyisobutylene (PIB) on the patterning surface and includes a 2 μm scale bar.

drop of PIB by aligning the center of the cantilever with the center of the reservoir drop and then performing a force-indentation experiment. After retracting from the surface, the thermal PSD was measured once more, revealing that both modes had shifted to lower frequencies with $\delta f_1 = 8.147$ kHz and $\delta f_2 = 21.056$ kHz (Figure 2a). With these measurements in hand, we solved eq 2 by equating m_l for $n = 1$ with m_l for $n = 2$ and numerically solving the resultant transcendental equation for x/L, which resulted in $x/L = 0.90105 \pm 0.00004$. This value was then used to find $m_l = 3.521 \pm 0.005$ ng.

In order to validate x determined by the cantilever bending model as an accurate measure of drop position, a series of experiments were conducted where x was compared to the position x_o measured by manual optical inspection (Figure 2b). Each cycle comprised bringing the probe in contact with a substrate to remove a fraction of the PIB, using a thermal PSD to determine δf_1 and δf_2, and subsequently measuring x_o/L using bright field optical microscopy. Here, x_o was estimated by measuring the distance between the center of the drop and the fixed end of the cantilever. Agreement between the drop position estimated by the two methods provided confidence in the interpretation of x. Interestingly, these experiments also show that as m_l decreases, x/L approaches 1, signifying that smaller drops move toward the free end of the cantilever (Figure 2c). We hypothesize that this is due to the 11° slope of the cantilever with respect to the surface, which results in the unpinned drop on the cantilever being moved toward the sample during retraction. This is an important feature for patterning as it indicates that the liquid drop will be able to contact the surface as it is depleted. Due to the shape of $N_1(x)$, the correction to m_l from the bending model decreases as the drop shrinks and moves toward the free end. This is reasonable considering that the mass-spring model effectively assumes that $x/L = 1$.

After showing that the cantilever bending model can accurately determine x, a series of experiments were conducted to evaluate whether it could accurately determine m_l. While the nonspherical shape of the drop made it challenging to accurately determine the volume of liquid on the probe, we hypothesized that by examining the mass decrease upon transferring liquid to a surface, it would be possible to compare the mass decrease and the volume of the written feature. Thus, we performed 62 liquid transfer operations in which the probe was brought into contact with a fluorosilane-coated silicon wafer. Prior to and immediately following each transfer operation, m_l was measured and the mass lost upon transfer was recorded as δm_l. After executing these transfer operations, each feature was characterized using optical microscopy and their diameter was estimated by fitting their perimeter to an ellipse. In order to estimate the volume V_o of these features using their diameters, the contact angle of micron-scale drops of PIB on fluorinated silicon was determined by inspecting a sample using a scanning electron microscope (SEM) (Figure 2d inset) to find a contact angle of 65 ± 3°. Using this value, V_o of each patterned feature was calculated by approximating each drop as a spherical cap. In agreement with the model, V_o and δm_l were highly correlated and fit to the relationship $\delta m_l = \rho V_0$ with $\rho = 985 \pm 4$ kg m^{-3}, in

https://doi.org/10.1021/acsami.1c00095
ACS Appl. Mater. Interfaces XXXX, XXX, XXX−XXX

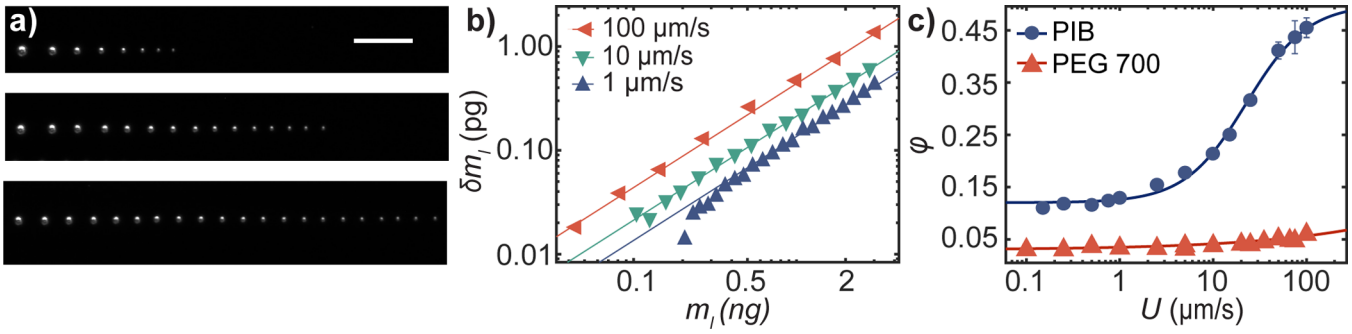

Figure 3. Establishing robust control over feature writing. (a) Optical micrographs showing written PIB features with (top) withdrawal speed $U = 100$ μm/s, (middle) $U = 10$ μm/s, and (bottom) $U = 1$ μm/s. Features were written from left to right, and the scale bar is 100 μm. (b) Measured δm_l vs m_l for the three experiments shown in (a) with the legend depicting U. Each data set was fit to $\delta m_l = \varphi m_l$ with transfer ratio φ. (c) Experimental φ vs U in the full range available to our AFM system. The curve is fit to an empirical transfer ratio model that is defined by three parameters, a dimensionless power law, a characteristic velocity, and the asymptotic φ at slow speeds. All data correspond to PIB and PEGDA written on a hydrophobic surface using 1 μm/s approach speed, 1 s dwell time, and 300 nN attractive setpoint.

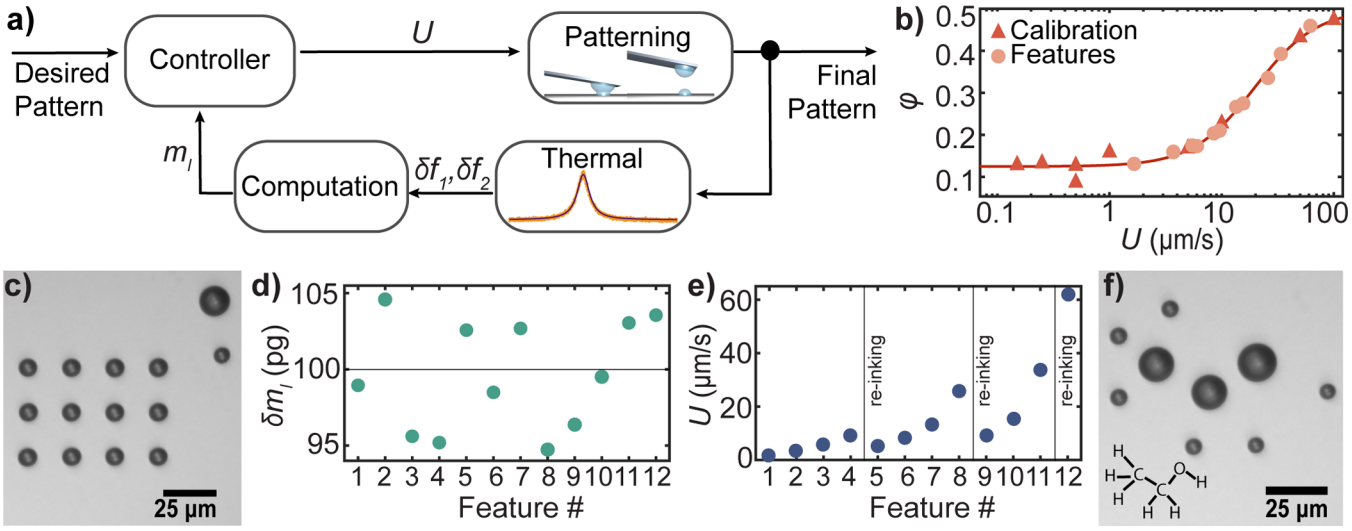

Figure 4. Preliminary closed-loop dip-pen nanolithography (DPN). (a) Block diagram for closed-loop DPN. A desired pattern is specified in the form of a list of feature locations and sizes. The controller then chooses a withdrawal speed U for the first feature, which is then patterned. Subsequently, a measurement of the thermal PSD is used to measure δf_1 and δf_2. These shifts are then used to compute m_l. This information is used to update the controller, and the cycle is continued until the pattern has been completely written. (b) Experimental φ vs U collected as part of an evaluation pattern. This includes 9 calibration features and 12 features written as part of the pattern. (c) Optical micrograph of the final pattern showing the 12 written features with two remaining liquid reservoirs in the top right. Scale bar is 25 μm. Features were written row-wise from the bottom right to the top left with the probe being re-inked in between features 4 and 5, between 8 and 9, and between 11 and 12. (d) Calculated δm_l of each feature. Here, the target feature size was 100 pg (e) Chosen U for each feature with re-inking events marked as gray lines. The large change in U between features is due to the algorithm accommodating the changing m_l. (f) Optical microscope image of patterning demonstration of a schematic of an ethanol molecule including two carbon atoms, one oxygen atom and six hydrogen atoms.

agreement with reported values for PIB that are in the range 950−1000 kg m^{-3}.[18,19]

Having a robust system to ensure contact between a liquid reservoir and a sample along with a validated method to measure δm_l indicates that liquid transport can be studied to determine its suitability as a patterning technique. In particular, one can consider a force−distance curve executed with a liquid-loaded probe as a liquid transfer operation where four major parameters are specified by the AFM software (Figure S4). In particular, the process is defined by the speed U_a at which the AFM probe approaches the substrate, the force value that signals the AFM to stop approaching, the dwell time t_d for which the probe is held in contact, and the retraction speed U. Taking inspiration from prior work on macroscale liquid transfer, we hypothesized that U is the most important property in determining the outcome of liquid patterning.[20−22] Thus, we utilize $U_a = 1$ μm s^{-1} to ensure that the cantilever was moving slowly enough that the 300 nN attractive force setpoint would be triggered when the liquid comes into contact with the surface and utilize $t_d = 1$ s to allow the capillary bridge equilibrate prior to retraction.

To study the effect of U on transport, we performed a series of experiments in which a probe was loaded with a single ∼3 ng drop of PIB and used to write a series of features with constant U (Figure 3a). In all cases, transport was observed with patterned features decreasing in size as the liquid drop on the probe was depleted. Interestingly, the number of features that a probe could write before being completely depleted varied, with faster U resulting in more rapid transport. In order to study the precise manner in which m_l and U together determine δm_l, we used inertial sensing to track the mass during these experiments

https://doi.org/10.1021/acsami.1c00095
ACS Appl. Mater. Interfaces XXXX, XXX, XXX−XXX

(Figure 3b). Interestingly, each series of features followed a monotonic curve that is well fit by the expression $\delta m_l = \varphi m_l$ where φ is a transfer ratio. Critically, this implies that in each writing cycle with a fixed U, a constant fraction of the liquid mass was transported to the substrate. This observation agrees with the understanding of macroscopic liquid transport[22−24] and has extremely important consequences for patterning as it means that the measured state of the probe system, namely, m_l, can be used to predict the outcome of a given transfer operation.

In order to further explore the liquid transport phenomena, we repeated the transport experiments using PIB for an additional 13 values of U between 0.15 and 100 μm s^{-1}, which corresponds to the full range available to our instrument. Strikingly, φ exhibited a smooth and monotonic increase with U from below 0.1 to nearly 0.5. This general trend is in good agreement with macroscopic liquid transport experiments between two plates where, at high velocities, bridge rupture is dominated by viscous forces and the liquid drop is divided in half,[20,25] while at low velocities, the relative contact angles of the two substrates determine the asymptotic value of φ.[26−28] Here, the higher contact angle of the fluorinated silicon substrate relative to the untreated probe indicates that surface tension works to drive the majority of the liquid back to the cantilever. Importantly, the velocity scale is set by the capillary number, which indicates that this transition should be shifted to higher values of U for less viscous liquids. Indeed, upon repeating these experiments with PEGDA, we found lower but gently increasing φ, indicating that the transition to capillary rupture dominated by viscous forces was not in the range of our instrument. A feature to emphasize is that the capillary number is only dependent upon speed and material properties, so the observed length scale-invariance of φ follows from the liquid phenomena.

From a patterning context, the ability to modulate the amount of liquid transported using a single control variable − here U − is very powerful as it indicates that one could construct a process by which features can be reliably and predictably patterned. From this perspective, we selected PIB as an ideal material for patterning using our instrument as it enabled us to vary φ by a factor of ∼5. In order to produce a functional form of $\varphi(U)$, we adopt an empirical relationship that had been previously used to describe macroscopic liquid transport,[22]

$$\varphi = 0.5 + \frac{\varphi_0 - 0.5}{1 + \left(\frac{U}{U_c}\right)^a}, \tag{3}$$

where the asymptotic transfer ratio φ_0, characteristic speed U_c, and power law scaling a are fitting parameters. Here, we find $\varphi_0 = 0.12 \pm 0.01$, $U_c = 23 \pm 2$ μm s^{-1}, and $a = 1.3 \pm 0.2$.

In order to explore the ability of this combination of probe architecture, liquid, and transfer prediction processes to realize closed-loop operation, we developed an iterative patterning process (Figure 4a). Acknowledging the fact that the details of transfer may depend on surface and environmental properties that may not be easily controlled (Figure S5); each patterning experiment should begin with an initial set of experiments to calibrate the transfer model (i.e., φ vs U). After calibration, a typical patterning cycle would comprise specifying a set of features in terms of their mass and location to be patterned under closed-loop control. To pattern each feature, U would be chosen based on m_l and the target δm_l. After writing this feature, a thermal PSD would be measured to obtain δf_1 and δf_2, simultaneously providing an estimate of the mass of liquid that was actually written. This information provides another U vs φ data point for updating the transfer model, which had initially been learned using the calibration features. This process of choosing the required U for the target mass and updating the transfer model based on measured mass of the patterned feature would be repeated for each additional feature until all the features in the set had been patterned. A critical feature of including the data in the transfer model in real-time is that it allows for performance to improve during the course of a patterning experiment or to adapt to potentially changing environmental conditions.

In an initial experiment to study patterning using this closed-loop process, we performed a patterning experiment to write an array of 100 pg PIB features in a square grid. Before writing these features, transfer experiments were performed with nine distinct U that were chosen to span the full speed range of our AFM. For each written calibration feature, φ was calculated and the initial transfer model was fit according to eq 3, resulting in $\varphi_0 = 0.12 \pm 0.01$, $U_c = 19 \pm 3$ μm s^{-1}, and $a = 1.5 \pm 0.3$. After calibration, the cantilever was reinked with $\delta m_l = 750$ pg of PIB for patterning. For the first feature with a target mass of 100 pg, the controller selected $U = 1.66$ μm s^{-1} with a target $\varphi = 0.13$. After the first feature was written, δm_l was calculated and used to update the transfer model. This process was repeated with U being iteratively chosen by the controller according to the updated transfer model and the current mass of ink on the cantilever. Prior to writing each feature, if the required φ for the target mass exceeded the maximum achievable φ (i.e., insufficient m_l), the probe was maneuvered above a PIB reservoir in the patterning canvas and reinked. At the end of the patterning experiments, with all 21 features included in the transfer model determination (Figure 4b), we found $\varphi_0 = 0.12 \pm 0.1$, $U_c = 20 \pm 5$ μm s^{-1}, and $a = 1.6 \pm 0.1$. The modest change between initial calibration and the conclusion of patterning validates the robustness of patterning using this method.

The nature of the closed-loop patterning experiment allowed us to evaluate it from a lithographic perspective. The result of this experiment was 12 features in a square grid with two reservoir droplets still visible at top right of the imaging area (Figure 4c). The features were written row-by-row from right to left starting from the bottom row. The *in situ* inertial sensing also produces a record of the mass of each feature (Figure 4d). The average mass of all 12 features was 99.6 pg with a standard deviation of 3.6 pg. From this, we compute the accuracy (difference from the target and the average) as 0.4% with a precision (spread about the average) of 4%. It is worth emphasizing that due to the scaling of diameter with volume, the precision with which this approach can dictate linear dimensions is therefore ∼1%. This performance compares favorably to prior efforts to quantify precision in DPN without feedback that have reported ∼5% variation in the feature radius under steady-state conditions, although it is worth emphasizing that prior approaches could not dial in a target feature size, so accuracy has not been a metric that could be quantified.[29,30]

A critical feature of this patterning process is that it was robust against adding addition ink to the probe. Specifically, three times during the patterning process, additional PIB had to be added to the cantilever. The effect of adding additional liquid is especially evident when examining the U value that was selected for each patterned feature (Figure 4e) as these were computed depending on m_l prior to writing and U increases as m_l decreases throughout the patterning process unless additional ink was

https://doi.org/10.1021/acsami.1c00095
ACS Appl. Mater. Interfaces XXXX, XXX, XXX−XXX

added. Critically, as inking occurred in a region that the probe could access while under piezoelectric control, adding additional material did not compromise registration accuracy. Moving to the reservoir and performing an inking operation take about the same amount of time as writing a single feature, since both of these are performed under piezoelectric control. The frequency of re-inking depended on the details of the pattern but typically occurred every 3−10 features, thus increasing the time required to write a given pattern by 10−30%. Furthermore, since the patterning fidelity was not degraded between inking cycles, the transfer calibration was therefore robust against any change in liquid quantity or wetting.

The fluid surface tension is an important parameter in determining the transport properties because it − together with the properties of the probe and patterning surfaces − determines the shape of the pendant drops and the asymptotic transfer ratio at the low velocity limit. While robust transfer was observed for all fluids studied, it is possible that patterning with fluids that have lower surface tension might be challenging on account of their lower contact angle. One route to address this potential problem would be to utilize vapor coating to lower the surface energy of the cantilever to maintain a high liquid contact angle.

It is important to emphasize that the geometry of the cantilever and its angle with respect to the patterning surface appear to ensure that special care is not needed when positioning a drop on the probe. Specifically, the 11° tilt toward the substrate − or perhaps the ability of the cantilever to bend toward the substrate when pulling a capillary bridge − means that the drop can slide down the cantilever toward the free end upon retraction. We hypothesize that this constitutes a self-correcting alignment effect where the drop is thus positioned in a protruding fashion to facilitate patterning. Additionally, an important feature of the two-harmonic mass sensing approach is that the position and mass of the liquid drop are both computed, allowing for an accurate determination of mass despite the drop not being pinned to a specific location.

In order to explore whether this closed-loop approach could be used to write more complex patterns with high fidelity, we designed a pattern that represents the molecular formula of ethanol (Figure 4f). In particular, we designated a series of dot features that each had target masses proportional to the atomic mass of carbon, oxygen, and hydrogen and resided in the positions that these atoms occupy in the molecular formula (Figure S6). The fidelity of this pattern shows the potential for this closed-loop DPN to control and modulate feature size and position and comprise a general patterning approach.

The resolution of the patterning process is dependent upon both the sensitivity of the cantilever to changes in mass and the precision with which the resonance frequency can be estimated. While it is challenging to determine the mass resolution without an independent process for measuring fluid transfer, it can be experimentally measured by comparing δm_l to V_o, although it is worth mentioning that estimating error in this way is highly conservative as it assumes that V_o is a perfect measure of drop volume. For the cantilever used herein evaluated using measurements of the thermal PSD interpreted with a two harmonic sensing scheme, we estimate a 2.4 pg resolution in mass sensing (Figure S7). Interestingly, repeating the same process utilizing a stiffer cantilever with an active tuning scheme revealed that 20 fg resolution is practical. In addition to validating the ability of this approach to pattern submicron features, this shows that advances in resonance frequency sensing and cantilever architecture could provide a path for further miniaturization.

3. CONCLUSIONS

The ability to specify a target feature size and adjust the patterning process under feedback control during an experiment is a critical feature that has previously been absent from DPN of fluids and other approaches for high-resolution patterning of fluids. While this work focused on a carefully chosen fluid−probe system that enables studying the fluid transport phenomena, the process is generalizable to many other systems with relevance to nanolithography and synthesis. As such, the closed-loop feedback enabled by this approach can be transformed into quantitative control over reagents for nanochemistry. While PIB was chosen as a polymeric fluid to study the fluid transfer process on account of its high viscosity, high surface tension, and low volatility, the only one of these three properties that is critical for quantitatively evaluating patterning is the low volatility. Indeed, many other polymeric fluids, including more complex ones such as block copolymers,[31] share this property and are thus amenable for patterning with feedback. Even those that are solids at room temperature can potentially be patterned at elevated temperatures provided they are thermoplastic.[32]

In this work, we demonstrated a novel method to perform closed-loop patterning with DPN of liquids to precisely control the mass of patterned features on the pL to sub-fL scales with resolution as good as 20 aL. Critically, realizing this required combining a tipless probe architecture, a rationally selected liquid for patterning, a novel two-harmonic inertial sensing approach, and a controller based upon a physical transport model. When combined, these approaches allow one to transport a predictable amount of liquid with better than 1% accuracy and ∼4% precision in terms of feature mass.

Recent efforts to enable the rapid determination of resonance frequencies with precision finer than possible with a PSD highlight the possibilities to further improve the precision and reduce the size of patterned features.[33] Given the high importance of preparing and manipulating liquid samples at ever finer scales in fields ranging from diagnostics to drug discovery, these results provide an important technical foundation to a new field of container-free chemistry with droplet-based nanoreactors.

4. EXPERIMENTAL SECTION

4.1. Materials. PIB (MW 1500 Da) was purchased from Polymer Source (Canada). PEGDA (Mn 700 Da) was purchased from Sigma Aldrich (USA). Si/SiO_x wafers (1−10 Ohm-cm, <100>, N doped with P) were purchased from University Wafers (USA).

4.2. Preparation of Hydrophobic Silicon Substrates. Smooth, hydrophobic substrates were prepared by functionalization of Si/SiO_x wafer chips with heptadecafluoro-1,1,2,2-tetrahydrodecyltrichlorosilane (FDTS). First, substrates were cleaned using bath sonication in acetone, sonication in isopropanol, and then blow drying under a nitrogen stream. After cleaning, the substrates were plasma treated (M4L RF Gas Plasma System, O_2 plasma at 500 mT, 500 W, 5 min). Substrates were placed in a vacuum chamber immediately after plasma treatment. Samples were left under vacuum with a small amount of FDTS for 3 h for vapor coating. Following the vapor coating, substrates were placed on a hotplate at 100 °C and baked for 10 min. Last, the substrates were cleaned using bath sonication in toluene and then in ethanol. The hydrophobicity of the substrates was confirmed by measuring their water contact angle, which was found to be ∼110°.

https://doi.org/10.1021/acsami.1c00095
ACS Appl. Mater. Interfaces XXXX, XXX, XXX−XXX

4.3. DPN Experiments. Patterning experiments were performed on a commercial AFM system (Asylum MFP-3D Infinity) under ambient conditions. NanoSensors tipless cantilevers (length 225 μm, width 28 μm, and nominal spring constant 2.8 N/m) were purchased from NanoAndMore (USA) and cleaned using bath sonication in toluene prior to experiments. In the beginning of the experiments, the cantilever was calibrated by performing a force−displacement curve on a silicon substrate to determine the optical lever sensitivity and then using a measurement of the thermal PSD to determine the spring constant and resonance frequencies. Prior to patterning experiments, a set of features with user-defined speed settings were patterned and the controller was trained by performing nonlinear least squares fitting to eq 3. Patterning conditions were selected by a closed-loop controller written in MATLAB, and resonance frequency measurements were determined by measuring the thermal PSD in between patterning operations.

4.4. Optical Microscopy and Image Analysis. Optical microscopy images were taken by using an Olympus BX43 microscope with a GS3-U3-120S6M-C Grasshopper camera, at 20× magnification with a resolution of 4240 × 2824 pixels. Image analysis was performed using ImageJ. Briefly, microscope images were converted to binary images using automated iterative thresholding. Particles were then identified by the software, and feature radii were determined using an elliptical fit to each feature. Feature volumes were calculated by using the spherical cap approximation method,[34]

$$V = \frac{\pi D^3}{24}\left(\frac{2 - 3\cos\theta + \cos^3\theta}{\sin^3\theta}\right) \quad (4)$$

where the base diameter D of the features was assumed to be circular with constant contact angle θ around its base. The contact angle of PIB on the hydrophobic silicon surface was measured using SEM and found to be $\theta = 65 \pm 3°$.

■ ASSOCIATED CONTENT

Supporting Information

The Supporting Information is available free of charge at https://pubs.acs.org/doi/10.1021/acsami.1c00095.

Discussion of drop dynamics on conical probes, calculation of the cantilever mass, discussion of capillary force during patterning and probe selection, details about liquid selection, analysis of variation of transfer properties, details of the molecule pattern, and supporting references (PDF)

■ AUTHOR INFORMATION

Corresponding Author

Keith A. Brown − *Department of Mechanical Engineering, Boston University, Boston, Massachusetts 02215, United States; Physics Department and Division of Materials Science and Engineering, Boston University, Boston, Massachusetts 02215, United States;* orcid.org/0000-0002-2379-2018; Email: brownka@bu.edu

Authors

Verda Saygin − *Department of Mechanical Engineering, Boston University, Boston, Massachusetts 02215, United States;* orcid.org/0000-0003-1835-4395

Bowen Xu − *Department of Mechanical Engineering, Boston University, Boston, Massachusetts 02215, United States;* orcid.org/0000-0002-3284-190X

Sean B. Andersson − *Department of Mechanical Engineering, Boston University, Boston, Massachusetts 02215, United States; Division of Systems Engineering, Boston University, Boston, Massachusetts 02215, United States;* orcid.org/0000-0001-7575-3507

Complete contact information is available at: https://pubs.acs.org/10.1021/acsami.1c00095

Notes

The authors declare no competing financial interest.

■ ACKNOWLEDGMENTS

This work was supported by the National Science Foundation (CMMI-1661412) and the Air Force Office of Scientific Research (FA9550-16-1-0150). We acknowledge support from the Boston University Photonics Center. We also thank Nourin Alsharif for assistance in taking SEM images.

■ REFERENCES

(1) Mayr, L. M.; Bojanic, D. Novel Trends in High-Throughput Screening. *Curr. Opin. Pharmacol.* **2009**, *9*, 580−588.

(2) Gorgulla, C.; Boeszoermenyi, A.; Wang, Z. F.; Fischer, P. D.; Coote, P. W.; Padmanabha Das, K. M.; Malets, Y. S.; Radchenko, D. S.; Moroz, Y. S.; Scott, D. A.; Fackeldey, K.; Hoffmann, M.; Iavniuk, I.; Wagner, G.; Arthanari, H. An Open-Source Drug Discovery Platform Enables Ultra-Large Virtual Screens. *Nature* **2020**, *580*, 663−668.

(3) Piner, R. D.; Zhu, J.; Xu, F.; Hong, S. Dip-Pen Nanolithography. *Science* **1999**, *283*, 661−664.

(4) Ivanisevic, A.; Mirkin, C. A. "Dip-Pen" Nanolithography on Semiconductor Surfaces. *J. Am. Chem. Soc.* **2001**, *123*, 7887−7889.

(5) Demers, L. M.; Ginger, D. S.; Park, S. J.; Li, Z.; Chung, S. W.; Mirkin, C. A. Direct Patterning of Modified Oligonucleotides on Metals and Insulators by Dip-Pen Nanolithography. *Science* **2002**, *296*, 1836−1838.

(6) Dawood, F.; Wang, J.; Schulze, P. A.; Sheehan, C. J.; Buck, M. R.; Dennis, A. M.; Majumder, S.; Krishnamurthy, S.; Ticknor, M.; Staude, I.; Brener, I.; Goodwin, P. M.; Amro, N. A.; Hollingsworth, J. A. The Role of Liquid Ink Transport in the Direct Placement of Quantum Dot Emitters onto Sub-Micrometer Antennas by Dip-Pen Nanolithography. *Small* **2018**, *14*, 1−10.

(7) Huang, L.; Braunschweig, A. B.; Shim, W.; Qin, L.; Lim, J. K.; Hurst, S. J.; Huo, F.; Xue, C.; Jang, J. W.; Mirkin, C. A. Matrix-Assisted Dip-Pen Nanolithography and Polymer Pen Lithography. *Small* **2010**, *6*, 1077−1081.

(8) Jang, J. W.; Zheng, Z.; Lee, O. S.; Shim, W.; Zheng, G.; Schatz, G. C.; Mirkin, C. A. Arrays of Nanoscale Lenses for Subwavelength Optical Lithography. *Nano Lett.* **2010**, *10*, 4399−4404.

(9) Hernandez-Santana, A.; Irvine, E.; Faulds, K.; Graham, D. Rapid Prototyping of Poly(Dimethoxysiloxane) Dot Arrays by Dip-Pen Nanolithography. *Chem. Sci.* **2011**, *2*, 211−215.

(10) Nakashima, H.; Higgins, M. J.; O'Connell, C.; Torimitsu, K.; Wallace, G. G. Liquid Deposition Patterning of Conducting Polymer Ink onto Hard and Soft Flexible Substrates via Dip-Pen Nanolithography. *Langmuir* **2012**, *28*, 804−811.

(11) Eichelsdoerfer, D. J.; Brown, K. A.; Mirkin, C. A. Capillary Bridge Rupture in Dip-Pen Nanolithography. *Soft Matter* **2014**, *10*, 5603−5608.

(12) O'Connell, C. D.; Higgins, M. J.; Sullivan, R. P.; Moulton, S. E.; Wallace, G. G. Ink-on-Probe Hydrodynamics in Atomic Force Microscope Deposition of Liquid Inks. *Small* **2014**, *10*, 3717−3728.

(13) O'Connell, C. D.; Higgins, M. J.; Marusic, D.; Moulton, S. E.; Wallace, G. G. Liquid Ink Deposition from an Atomic Force Microscope Tip: Deposition Monitoring and Control of Feature Size. *Langmuir* **2014**, *30*, 2712−2721.

(14) Biswas, S.; Hirtz, M.; Fuchs, H. Measurement of Mass Transfer during Dip-Pen Nanolithography with Phospholipids. *Small* **2011**, *7*, 2081−2086.

(15) Farmakidis, N.; Brown, K. A. Quantifying Liquid Transport and Patterning Using Atomic Force Microscopy. *Langmuir* **2017**, *33*, 5173−5178.

(16) McCarthy, J.; Vella, D.; Castrejón-Pita, A. A. Dynamics of Droplets on Cones: Self-Propulsion Due to Curvature Gradients. *Soft Matter* **2019**, *15*, 9997−10004.

(17) Dohn, S.; Svendsen, W.; Boisen, A.; Hansen, O. Mass and Position Determination of Attached Particles on Cantilever Based Mass Sensors. *Rev. Sci. Instrum.* **2007**, *78*, 2005−2008.
(18) Ferry, J. D.; Parks, G. S. Viscous Properties of Polyisobutylene. *J. Appl. Phys.* **1935**, *6*, 356−362.
(19) Eichinger, B. E.; Flory, P. J. Determination of the Equation of State of Polyisobutylene. *Macromolecules* **1968**, *1*, 285−286.
(20) Kang, H. W.; Sung, H. J.; Lee, T. M.; Kim, D. S.; Kim, C. J. Liquid Transfer between Two Separating Plates for Micro-Gravure-Offset Printing. *J. Micromech. Microeng.* **2009**, *19*, 015025.
(21) Bai, S. E.; Shim, J. S.; Lee, C. H.; Bai, C. H.; Shin, K. Y. Dynamic Effect of Surface Contact Angle on Liquid Transfer In a Low Speed Printing Process. *Jpn. J. Appl. Phys.* **2014**, *53*, No. 05HC05.
(22) Chen, H.; Tang, T.; Amirfazli, A. Effects of Surface Wettability on Fast Liquid Transfer. *Phys. Fluids* **2015**, *27*, No. 112102.
(23) Huang, W. X.; Lee, S. H.; Sung, H. J.; Lee, T. M.; Kim, D. S. Simulation of Liquid Transfer between Separating Walls for Modeling Micro-Gravure-Offset Printing. *Int. J. Heat Fluid Flow* **2008**, *29*, 1436−1446.
(24) Huang, C. H.; Carvalho, M. S.; Kumar, S. Stretching Liquid Bridges with Moving Contact Lines: Comparison of Liquid-Transfer Predictions and Experiments. *Soft Matter* **2016**, *12*, 7457−7469.
(25) Chadov, A. V.; Yakhnin, E. D. Investigation of the Transfer of a Liquid from One Surface to Another 2. Dynamic Transfer. *Kolloidn. Zh.* **1983**, *2*, 1183.
(26) Chadov, A. V.; Yakhnin, E. D. Investigation of the Transfer of a Liquid from One Surface to Another 1. Slow Transfer Method of Approximate Calculation. *Kolloidn. Zh.* **1979**, *41*, 817.
(27) Chen, H.; Tang, T.; Amirfazli, A. Liquid Transfer Mechanism between Two Surfaces and the Role of Contact Angles. *Soft Matter* **2014**, *10*, 2503−2507.
(28) Chen, H.; Tang, T.; Zhao, H.; Law, K. Y.; Amirfazli, A. How Pinning and Contact Angle Hysteresis Govern Quasi-Static Liquid Drop Transfer. *Soft Matter* **2016**, *12*, 1998−2008.
(29) Liao, X.; Braunschweig, A. B.; Zheng, Z.; Mirkin, C. A. Force- and Time-Dependent Feature Size and Shape Control in Molecular Printing via Polymer-Pen Lithography. *Small* **2010**, *6*, 1082−1086.
(30) Eichelsdoerfer, D. J.; Brown, K. A.; Wang, M. X.; Mirkin, C. A. Role of Absorbed Solvent in Polymer Pen Lithography. *J. Phys. Chem. B* **2013**, *117*, 16363−16368.
(31) Liu, G.; Zhou, Y.; Banga, R. S.; Boya, R.; Brown, K. A.; Chipre, A. J.; Nguyen, S. B. T.; Mirkin, C. A. The Role of Viscosity on Polymer Ink Transport in Dip-Pen Nanolithography. *Chem. Sci.* **2013**, *4*, 2093−2099.
(32) Sheehan, P. E.; Whitman, L. J.; King, W. P.; Nelson, B. A. Nanoscale Deposition of Solid Inks via Thermal Dip Pen Nanolithography. *Appl. Phys. Lett.* **2004**, *85*, 1589−1591.
(33) Kang, Z.; Saygin, V.; Brown, K. A.; Andersson, S. A Stepped-Sine Curve-Fit Algorithm for Finding Cantilever Resonance Shifts in AFM. *Proc. Am. Control Conf.* **2019**, 4368−4373.
(34) ElSherbini, A. I.; Jacobi, A. M. Liquid Drops on Vertical and Inclined Surfaces: I. An Experimental Study of Drop Geometry. *J. Colloid Interface Sci.* **2004**, *273*, 556−565.

https://doi.org/10.1021/acsami.1c00095
ACS Appl. Mater. Interfaces XXXX, XXX, XXX−XXX